Three-Dimensional Vortices Generated by Self-Replication in Stably Stratified Rotating Shear Flows

Philip S. Marcus,* Suyang Pei, Chung-Hsiang Jiang, and Pedram Hassanzadeh
Department of Mechanical Engineering, University of California, Berkeley, California 94720, USA
(Received 30 September 2012; revised manuscript received 17 March 2013; published 20 August 2013)

A previously unknown instability creates space-filling lattices of 3D vortices in linearly stable, rotating, stratified shear flows. The instability starts from an easily excited critical layer. The layer intensifies by drawing energy from the background shear and rolls up into vortices that excite new critical layers and vortices. The vortices self-similarly replicate to create lattices of turbulent vortices. The vortices persist for all time. This self-replication occurs in stratified Couette flows and in the dead zones of protoplanetary disks where it can destabilize Keplerian flows.

DOI: 10.1103/PhysRevLett.111.084501 PACS numbers: 47.20.Ft, 47.20.Pc, 47.55.Hd, 97.10.Bt

Introduction.—For a protostar to accrete gas from its protoplanetary disk (PPD) and form a star, the PPD must be unstable and transport angular momentum outward [1]. This has led to efforts to find instabilities in PPDs and other rotating flows that satisfy Rayleigh's criterion for centrifugal stability; i.e., the absolute value of angular momentum increases with increasing radius [2]. Numerical studies [3,4] of PPDs and experimental studies [5] of rotating flows where the velocity obeys Rayleigh's criterion confirm the stability of these flows (although there are recent controversies [6–8]). In a PPD where the gas is sufficiently ionized to couple to magnetic fields, the magnetorotational instability (MRI) [1] operates. However, large regions of PPDs, known as dead zones, are too cool and un-ionized to have magnetorotational instability. Other instabilities [9,10] could destabilize a PPD, but they require unrealistic boundaries or continually forced perturbations. Thus, star formation remains problematic.

Here we report a new finite-amplitude instability in rotating, stratified, shearing flows in Cartesian or cylindrical geometries with velocities that would satisfy Rayleigh's stability criterion if the densities were constant (as assumed by Rayleigh). We examine rotating plane Couette flow, which is the canonical test for PPD stability. In previous studies using ideal gases [1,3,4], these plane Couette flow PPD models were stable, but they were all initialized with no vertical density gradient and no vertical gravity g. In contrast, here we include a stably stratified initial density ρ with $g \neq 0$ (as in a PPD). Previously, we observed, but did not understand, an instability in a PPD with an ideal gas and $g \neq 0$ [11,12]. Thus, to understand the instability, here we consider a Boussinesq fluid with constant g. The 3D vortices found here are unique: a vortex that grows from a single, small-volume, initial perturbation triggers a 1st generation of vortices nearby. This 1st generation of vortices grows and triggers a 2nd generation. The triggering of subsequent generations continues *ad infinitum*. The vortices do not advect in the cross-stream direction, but the front dividing the vortex-populated fluid from the unperturbed fluid does. (Figs. 1 and 2.) Because the vortices grow large and spawn new generations that march across the domain of a dead zone, we refer to vortices that self-replicate to fill the domain as zombie vortices.

The unperturbed velocity of plane Couette flow observed in a frame with angular velocity $\Omega\hat{\mathbf{z}} \equiv f/2\hat{\mathbf{z}}$ is $\bar{\mathbf{v}} = \bar{V}(x)\hat{\mathbf{y}}$ with $\bar{V}(x) \equiv \sigma x$, where σ is the uniform shear, and x and y are the cross-stream and streamwise coordinates. "Hatted" quantities are unit vectors. The unperturbed density is $\bar{\rho}(z) = \rho_0(1 - \bar{N}^2 z/g)$, where ρ_0 is constant and $\bar{N} \equiv \sqrt{-g(d\bar{\rho}/dz)/\rho_0}$ is the initial

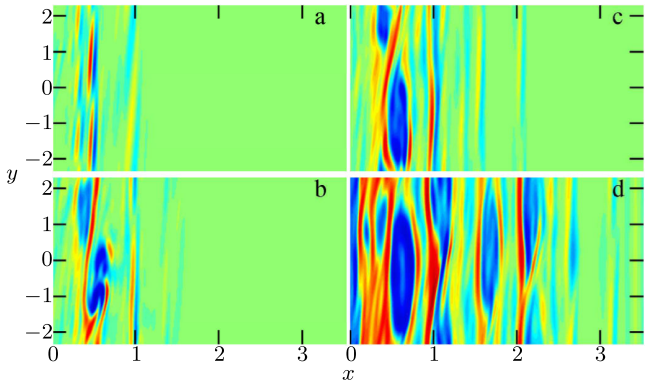

FIG. 1 (color online). $\omega_z/f \equiv$ Ro of the anticyclonic (blue) vortices and cyclonic (red) vortex layers in the x-y plane. The initial perturbing vortex at the origin is above the plane shown here ($z = -0.4$). The first generation zombie vortices form at $|x| \leq 1$, and sweep outward in x. The Rossby number Ro of these vortices is ~ -0.2. (The color is reddest at $\omega_z/f = 0.2$, e.g., near $x = 1/3$ at the bottom of panel d; bluest at $\omega_z/f = -0.2$, e.g., near $x = 0.6$ in panel d; and green at $\omega_z/f = 0$). $f/\bar{N} = 1$ and $\sigma/\bar{N} = -3/4$. The x-y domain is $|x| \leq 4.7124$; $|y| \leq 2.3562$, and is larger than shown. Movies of Figs. 1 and 2 are in the Supplemental Material [25]. (a) $t = 64/\bar{N}$. (b) $t = 256/\bar{N}$. (c) $t = 576/\bar{N}$. (d) $t = 2240/\bar{N}$. See text for details.

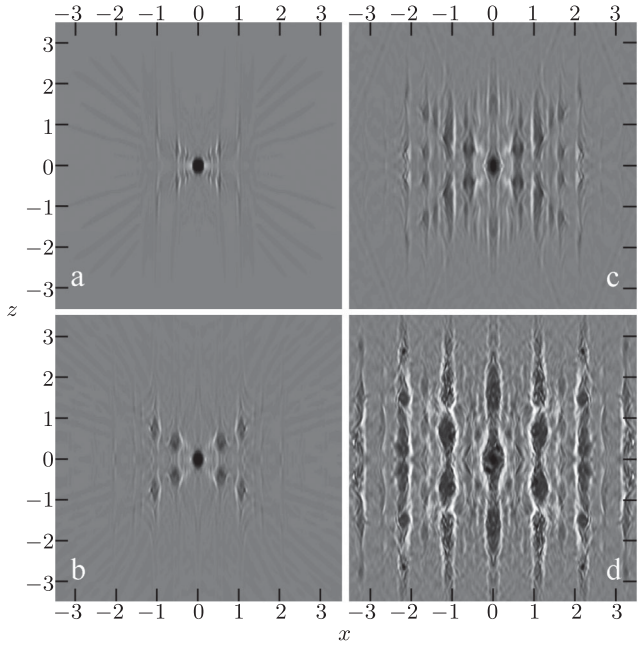

FIG. 2. Zombie vortices sweep outward from the perturbing vortex at the origin in the x-z plane (at $y = 0$). Anticyclonic ω_z is black (darkest is $\omega_z/f = -0.2$) and cyclonic is white (lightest is $\omega_z/f = 0.2$). This is the same flow as in Fig. 1. The domain has $|z| \le 4.7124$ and is larger than shown. (a) $t = 128/\bar{N}$. Critical layers with $s = 0$ and $|m| = 1$, 2, and 3 are visible. Diagonal lines are internal inertio-gravity waves with shear, not critical layers. (b) $t = 480/\bar{N}$. 1st generation vortices near $|x| = 1$ and 1/2 have rolled up from critical layers with $s = 0$ and $|m| = 1$ and 2, respectively. (c) $t = 1632/\bar{N}$. 2nd generation $|m| = 1$ vortices near $|x| = 0$ and 2 were spawned from the 1st generation vortices near $|x| = 1$. Another 2nd generation of $|m| = 1$ vortices is near $|x| \simeq 1/2$ and 3/2, which were spawned by the 1st generation near $|x| = 1/2$. (d) $t = 3072/\bar{N}$. 1st, 2nd, and 3rd generation vortices.

unperturbed Brunt-Väisälä frequency. In the rotating frame, the governing equations are

$$\partial \mathbf{v}/\partial t = -(\mathbf{v}\cdot\nabla)\mathbf{v} - \frac{\nabla\Pi}{\rho_0} + f\mathbf{v}\times\hat{\mathbf{z}} - \frac{(\rho-\rho_0)g}{\rho_0}\hat{\mathbf{z}}, \quad (1)$$

$$\partial\rho/\partial t = -(\mathbf{v}\cdot\nabla)\rho, \quad (2)$$

$$\nabla\cdot\mathbf{v} = 0, \quad (3)$$

where Π is the pressure head. When Eqs. (1)–(3) are linearized about $\bar{V}(x)$ and $\bar{\rho}(z)$, the eigenmodes are proportional to $e^{i(k_y y + k_z z - st)}$. When the initial density $\bar{\rho}$ is stably stratified or constant, plane Couette flow is neutrally linearly stable (i.e., s is real, and eigenmodes neither grow nor decay).

Critical layers.—The eigenequation for the eigenmodes of Eqs. (1)–(3) is a generalization of Rayleigh's equation [13] and is a 2nd-order ordinary differential equation. The coefficient of the highest-derivative term is

$$[\bar{V}(x) - s/k_y]\{[\bar{V}(x) - s/k_y]^2 - (\bar{N}/k_y)^2\}. \quad (4)$$

Eigenmodes of an ordinary differential equation are singular at locations x^* where the coefficient of the highest-derivative term is zero. There they form critical layers [13]. For fluids with constant density, critical layers obey $\bar{V}(x^*) = s/k_y$. We refer to these as barotropic critical layers. For $\bar{N} \neq 0$, expression (4) shows that there are eigenmodes with barotropic critical layers, but our computations show that they are difficult to excite and never form vortices. However, there is another class of eigenmodes with critical layers; they have $\bar{V}(x^*) - s/k_y \pm \bar{N}/k_y = 0$, and we call them baroclinic critical layers. Weak baroclinic critical layers were shown to exist in nonrotating, stratified flows [14], but we believe that this is the first study of these layers in flows with f, $\bar{N}$, and $|\sigma|$ of the same order (as near the midplane of a PPD). With anticyclonic shear ($f\sigma < 0$), as in a PPD, all of our calculations with $\bar{N} \simeq f \simeq |\sigma|$ fill the domain with zombie vortices when the initial finite-amplitude perturbation is sufficiently large (see below). To verify our computations, flows were computed with two independent codes. At the x boundaries, one code enforced an outward-going wave condition, and the other used the shearing sheet approximation [15]. The codes produced similar results.

We show that the new finite-amplitude instability works by first creating large-amplitude vortex layers at the critical layers. The curl of Eq. (1) gives

$$\partial\omega_z/\partial t = -(\mathbf{v}\cdot\nabla)\omega_z + (\boldsymbol{\omega}\cdot\nabla)v_z + (f+\sigma)(\partial v_z/\partial z), \quad (5)$$

where $\boldsymbol{\omega}$ is the relative vorticity $\boldsymbol{\omega} \equiv \nabla\times(\mathbf{v} - \bar{V}(x)\hat{\mathbf{y}})$. Vortex layers form at baroclinic critical layers because the z component of the velocity v_z of the neutrally stable eigenmode is singular there. Equation (5) shows that the generalized Coriolis term $(f+\sigma)(\partial v_z/\partial z)$ creates ω_z. Within the baroclinic critical layer, the singular $\partial v_z/\partial z$ is nearly antisymmetric about $x = x^*$; on one side of the layer $v_z \to \infty$, and on the other $v_z \to -\infty$; thus, the last term in Eq. (5) creates a large-amplitude vortex layer centered at x^* made of dipolar segments with one side cyclonic ($\omega_z f > 0$) and the other anticyclonic ($\omega_z f < 0$) [c.f. Fig. 1(a)]. Barotropic critical layers do not form vortex layers; although their eigenmodes' v_y is singular, v_z is everywhere finite. From this point on, we use nondimensional units with the units of time $1/\bar{N}$ and length $|(L\bar{N})/(2\pi\sigma)|$, where L is the periodicity length in y. Thus, k_y in expression (4) is $2\pi m/L$, where m is an integer. Baroclinic critical layers have $k_y \neq 0$, and expression (4) shows that they are at

$$x^* = -(s \pm 1)/m. \quad (6)$$

Equations (1)–(3) and their boundary conditions are invariant under translations in y and z, and also under translation in x by δ when accompanied by a streamwise boost in

velocity of $\sigma\delta$. The latter symmetry is shift-and-boost symmetry, c.f. [16,17], and is the basis of the shearing sheet boundary conditions [1,15]. Because of the shift-and-boost symmetry, the origin of the x axis is not unique, so Eq. (6) has the following meaning: x^* is the cross-stream distance between a perturbation and the location of the baroclinic critical layer that it excites.

Many types of perturbations create zombie vortices. Most relevant to PPDs is a Kolmogorov spectrum of noise where the velocity and Rossby number $\mathrm{Ro} \equiv \omega_z/f$ of the initial eddies scale, respectively, as $l^{1/3}$ and $l^{-2/3}$, where l is the eddy diameter. The smallest eddies have the largest vorticity and Ro. In calculations with $\sigma/f = -3/4$ and $0.5 \leq \bar{N}/f \leq 1$ (the regions we explored in a PPD [11]), regardless of how small we make the amplitude of the initial Kolmogorov energy spectrum, if the spatial resolution is sufficient, the smallest eddies have a sufficiently large $|\mathrm{Ro}|$ to trigger the instability and create zombie vortices. The vortices eventually fill the domain, such that at late times the volume they occupy is of order of the domain's volume. To better understand zombie vortex formation and replication, we simulated flows with $\sigma/f = -3/4$ and $0.5 \leq \bar{N}/f \leq 1$ initialized with a single "shielded" [18] anticyclone at the origin. These initial conditions produced flows filled with zombie vortices with $-0.35 < \mathrm{Ro} < -0.15$ when the initial anticyclone had $|\mathrm{Ro}| \gtrsim 0.2$. Figures 1 and 2 illustrate the case where the initial anticyclone has $\mathrm{Ro} = -0.31$ (as in the PPD where we first observed zombie vortices [11]) and volume $\sim 10^{-4}$ of the domain. The velocity perturbation due to the initial vortex is significant only near the origin and is small, $\sim 10^{-2}\sigma L_x$, where L_x is the domain size in x. (Velocity perturbations in PPD studies are considered small when they are less than $\sim 0.1\sigma L_x$ [3].) Our initial vortex is in quasiequilibrium as in [11] such that Eqs. (1) and (3), but not (2), are in approximate steady equilibrium. The initial density perturbation is confined to the initial vortex. Equation (2) allows ρ and $N(x, y, z, t)$ to change. Figure 1 shows ω_z in an x-y plane. The perturbing vortex is nearly steady, so it excites critical layers with frequencies $s = 0$. Thus, Eq. (6) shows that the critical layers are at $|x^*| = 1/|m|$ with no critical layers at $|x| > 1$. Figure 1(a) shows vortex layers at these critical layers: ω_z appears at $x = 1/|m|$ as $|m|$ segments of dipolar stripes aligned in the streamwise y direction for $|m| = 1$, 2, and 3. A Fourier analysis shows that the stripes have $s = 0$. We previously showed [19,20] that in shear flows with $f\sigma < 0$, cyclonic vortex layers aligned in the streamwise direction are stable, whereas anticyclonic layers are unstable, roll up into discrete anticyclones, and merge to form one large anticyclone. This behavior is seen in Fig. 1(b). The anticyclonic vorticity at $x = 1/3$ has rolled up and merged into a single anticyclone (near $y = 1.5$). The anticyclonic vorticity at $x = 1/2$ has rolled up into an anticyclone near $y = -0.5$. In contrast, the cyclonic vorticity near $x = 1/2$ has formed a continuous, meandering filament. At later times [Fig. 1(c)] the anticyclones near $x = 1/3$ (and near $y = 2$) and near $x = 1/2$ (and near $y = -1$) have become larger. Figures 1(c) and 1(d) show critical layers and vortices at $|x| > 1$, which cannot be created by perturbations at the origin. The layers at $|x| > 1$ are due to the self-replication of 1st generation vortices at $|x| \leq 1$. A vortex at *any* location will excite critical layers in a manner exactly like the original perturbing vortex due to the shift-and-boost symmetry (and will have $s = 0$ when viewed in the frame moving with the perturbing vortex). Figure 1(c) shows 2nd generation critical layers at $x = 4/3$, $3/2$, 2, and $2/3$, all with $|m| = 1$ and excited by 1st generation vortices at $x = 1/3$, $1/2$, 1, and $-1/3$, respectively. Figure 1(d) shows 3rd generation critical layers at $2 < x \leq 3$ and 4th generation critical layers forming at $x > 3$. At later times the vortices from $|m| = 1$ critical layers dominate [Fig. 2(d)]. At very late times, the vortices have cross-stream diameters of order unity (see below). Within each zombie vortex the density mixes so that it is in accord with its near hydrostatic and cyclogeostrophic equilibrium (c.f. [18]). However, there is horizontal, but very little vertical, mixing of density outside the vortices, so the background vertical density stratification and N remain within 1% of their initial unperturbed values. The lack of vertical mixing, despite strong horizontal mixing, was seen in our earlier simulations [11] and laboratory experiments [21] of vortices in rotating, stratified flows.

Figure 2 shows the flow in Fig. 1 viewed in the x-z plane and illustrates our main result: at late times the domain fills with anticyclones. Because the initial flow is homogeneous with uniform σ and $\bar{N}$, the vortices form a regular lattice despite the flow's turbulence. As time progresses in Fig. 2, the vortex population spreads out from the perturbing vortex at the origin. At early times [Fig. 2(a)], the flow has 1st generation critical layers, with $|m| = 1$, 2, and 3 being most apparent. In this first generation, and all subsequent generations, a vortex perturbs the flow and creates four new prominent vortices at its $|m| = 1$ critical layers at locations in x that are $\pm l_x$ distant from itself and at locations in z that are $\pm l_z$ distant from itself. (l_x is physically set by, and equal to, the distance in x from a perturbing vortex to the anticyclonic piece of the vortex layer formed by its $|m| = 1$ critical layer; this distance is slightly greater than unity.) The 2nd generation $m = 1$ critical layers created by the 1st generation vortices with $|m| = 1$, 2, and 3 are faintly visible in Fig. 2(b) and much more so in Fig. 2(c). At later times [Fig. 2(d)], the $|m| = 1$ vortices descended from the 1st generation $|m| = 1$ vortices dominate and form a lattice of zombie vortices located at $[x = 2nl_x, z = 2jl_z]$ and at $[x = (2n + 1)l_x, z = (2j + 1)l_z]$, for all integers n and j.

The characteristic $|\mathrm{Ro}|$ of late-time zombie vortices in Figs. 1 and 2 is ~ 0.2, consistent with zombie vortices in flows initialized with noise. After a vortex forms, its $|\mathrm{Ro}|$

intensifies to its approximate peak value within a few of its turnaround times, and it remains near that value indefinitely. Based on several numerical experiments, it appears that the late-time values of |Ro| depend on the parameters $\bar{N}$, f, and σ rather than on properties of the initial perturbation. To examine the energy of the vortices and discover its source, we decomposed the flow's energy into two orthogonal parts: (1) the zonal component consisting of the kinetic energy of the streamwise velocity component with Fourier modes $k_z = k_y = 0$ (i.e., the background shearing flow), and (2) the nonzonal component consisting of everything else, including the potential energy $g \int z(\rho - \bar{\rho})$ ($d$volume). If the initial flow were unperturbed, then the initial energy would be all zonal. In the flow in Figs. 1 and 2, there is a small initial nonzonal component due to the initial vortex at the origin. At later times, the nonzonal component represents the energy of the initial vortex and the zombie vortices (and turbulence and waves). The nonzonal energy initially increases superexponentially for $0 \leq t \lesssim 190$, increasing to $\sim$15 times its initial value. Then, the nonzonal energy increases approximately exponentially with an e-folding time of $\sim$860, such that at $t = 3072$ in Fig. 2(d) the nonzonal energy is more than 400 times its initial value. The energy increase in the nonzonal component is supplied by the zonal energy. The exponential growth of the nonzonal energy is due to the fact that vortices in the vortex-populated region grow exponentially in size, and not due to a long-term exponential increase of the velocity of each zombie vortex. Therefore, the nonzonal energy must plateau once the vortices fill the domain. If the self-replication were self-similar, we would expect the perimeter of the front between the vortex-populated flow and unperturbed flow in each x-z plane to grow as t and the number of vortices to increase as t^2, which is consistent with our calculations.

Discussion.—We have shown that linearly, neutrally stable plane Couette flow becomes finite-amplitude unstable when it is vertically stably stratified. In the example here, baroclinic critical layers are excited by a small vortex, but our calculations show that a variety of small-volume, small-energy perturbations cause critical layers to grow and roll up into large-volume, large-energy vortices. In general, this instability self-replicates with each new vortex exciting new layers that roll up until the domain fills with compact 3D (i.e., not Taylor columns) vortices. The robustness of zombie vortices is evident from the fact that they survive indefinitely even though they are embedded in a turbulent flow at late times. They survive by drawing energy from the background shear flow. For constant $\bar{N}$ and σ, the unperturbed flow is homogeneous, and vortex self-replication is self-similar with zombie vortices forming a regular lattice. The regularity of the lattice allows for reinforcement: each vortex reexcites four other vortices in the lattice, and each vortex in the lattice is continually reexcited by four other vortices. Zombie vortices occur frequently in our simulations of Boussinesq and compressible fluids, so they pose a paradox: if they are so common, why have they not been reported earlier? We believe there are three reasons: (1) instabilities have not been systematically sought in stratified Couette flows [9]; (2) with few exceptions [22], stability studies of ideal gases in PPDs were carried out with no initial vertical stratification [3,4]; and (3) the necessary spatial resolution to compute critical layers is lacking in many calculations. Zombie vortices occur in our calculations of the dead zones of protoplanetary disks [11], which suggests that they may have an important role in star and planet formation. In addition, zombie vortices should be observable in laboratory circular Couette flows with stratified salt water for parameter values where the flow is linearly stable with respect to centrifugal instability [13], stratorotational instability (SRI) [9,23], and other instabilities [24].

We thank NSF-XSEDE, NASA-HEC, NASA-PATM, NSF-ATI, and NSF-AST for support.

*pmarcus@me.berkeley.edu

[1] S. A. Balbus and J. F. Hawley, Rev. Mod. Phys. **70**, 1 (1998).
[2] Lord Rayleigh, Proc. R. Soc. A **93**, 148 (1917).
[3] S. A. Balbus, J. F. Hawley, and J. M. Stone, Astrophys. J. **467**, 76 (1996).
[4] Y. Shen, J. M. Stone, and T. A. Gardiner, Astrophys. J. **653**, 513 (2006).
[5] H. Ji, M. Burin, E. Schartman, and J. Goodman, Nature (London) **444**, 343 (2006).
[6] M. S. Paoletti, D. M. S. van Gils, B. Dubrulle, C. Sun, D. Lohse, and D. P. Lathrop, Astron. Astrophys. **547**, A64 (2012).
[7] E. Schartman, H. Ji, M. J. Burin, and J. Goodman, Astron. Astrophys. **543**, A94 (2012).
[8] M. Avila, Phys. Rev. Lett. **108**, 124501 (2012).
[9] M. Le Bars and P. Le Gal, Phys. Rev. Lett. **99**, 064502 (2007).
[10] R. V. E. Lovelace, H. Li, S. A. Colgate, and A. F. Nelson, Astrophys. J. **513**, 805 (1999).
[11] J. A. Barranco and P. S. Marcus, Astrophys. J. **623**, 1157 (2005).
[12] P. S. Marcus, C.-H. Jiang, S. Pei, and P. Hassanzadeh, Eur. Phys. J. Web Conf. **46**, 03 006 (2013).
[13] P. G. Drazin and W. Reid, *Hydrodynamic Stability* (Cambridge University Press, Cambridge, England, 1981).
[14] N. Boulanger, P. Meunier, and S. Le Dizès, J. Fluid Mech. **583**, 443 (2007).
[15] J. A. Barranco and P. S. Marcus, J. Comput. Phys. **219**, 21 (2006).
[16] P. Goldreich and D. Lynden-Bell, Mon. Not. R. Astron. Soc. **130**, 125 (1965).
[17] P. S. Marcus and W. H. Press, J. Fluid Mech. **79**, 525 (1977).
[18] P. Hassanzadeh, P. S. Marcus, and P. Le Gal, J. Fluid Mech. **706**, 46 (2012).
[19] P. S. Marcus, J. Fluid Mech. **215**, 393 (1990).

[20] P. S. Marcus, Annu. Rev. Astron. Astrophys. **31**, 523 (1993).
[21] O. Aubert, M. Le Bars, P. Le Gal, and P. S. Marcus, J. Fluid Mech. **706**, 34 (2012).
[22] A. G. Tevzadze, G. D. Chagelishvili, and J. P. Zahn, Astron. Astrophys. **478**, 9 (2008).
[23] M. J. Molemaker, J. C. McWilliams, and I. Yavneh, Phys. Rev. Lett. **86**, 5270 (2001).
[24] S. Le Dizès and P. Billant, Phys. Fluids **21**, 096602 (2009).
[25] See Supplemental Material at http://link.aps.org/supplemental/10.1103/PhysRevLett.111.084501 for movies of Figs. 1 and 2.